Journal of Operation and Automation in Power Engineering
Vol. 2, No. 2, Summer & Fall 2014, Pages: 121-128
http://joape.uma.ac.ir

Experimental and 3D Finite Element Analysis of a Slotless Air-Cored Axial Flux PMSG for Wind Turbine Application

V. Behjat*, A. R. Dehghanzadeh
Department of Electrical Engineering, Azarbaijan Shahid Madani University, Tabriz, Iran

ABSTRACT
In this research paper, the performance of an air-cored axial flux permanent magnet synchronous generator is evaluated for low speed, direct drive applications using 3D finite element modeling and experimental tests. The structure of the considered machine consists of double rotor and coreless stator, which results in the absence of core losses, reduction of stator weight and elimination of cogging torque. In addition, the generator output voltage is sinusoidal in low speed operation and has a linear relationship with rotor speed, which makes it a suitable option for wind turbine applications. The simulation results of the proposed generator coincide very well with the experimental results on a system realized in the laboratory.

KEYWORDS: Axial flux permanent magnet synchronous generator, Air-cored, 3D finite element analysis, Wind turbine.

1. INTRODUCTION

Growing environmental concerns and attempts to decrease dependency on fossil fuel sources are bringing renewable energy resources to the tendency of the electrical power sector [1]. Wind power is one of the renewable energies received more attention due to its clean and economical advantages. It is predicted that by 2020 up to 12% of the world's electrical energy will be supplied by wind turbine [2].

Wind turbines are categorized into two classes: fixed speed and variable speed. Nowadays, variable speed wind turbines have become more universal than traditional fixed speed turbines because of the more efficient energy production, enhanced power quality and improved dynamic performance during grid disturbances [3,4]. In addition, mechanical stresses can be decreased in variable speed wind turbines respect to fix ones [5]. Variable speed wind turbines use different generators such as: variable-speed doubly fed induction generator, which utilizes a frequency converter between the rotor windings and the grid; and variable-speed synchronous generator, which is either a wound rotor synchronous generator or a Permanent-Magnet Synchronous Generator (PMSG). Synchronous generators provide great flexibility to meet different technical requirements with power ratings from a few kilowatts to a few megawatts in wind turbine applications [6]. PMSG can be designed with a large number of poles and directly coupled with the turbine. As a result, installation and maintenance costs are reduced and provide an advantage over Induction Generator (IG) based turbines where a gearbox is an essential component of the system.

Permanent Magnet (PM) generators are classified into radial-flux and Axial-Flux (AF) machines, in view of the flux direction. As compared to traditional radial flux machines, the AF machines show innate and useful modularity features and can achieve higher power density levels, particularly if a high number of poles are considered. On the other hand, in the case of distributed windings, it is difficult to achieve a high pole number. In fact, in order to secure a minimum possible size of the tooth pitch, reduction of the number q of slots (pole phase) is

Received: 16 May 2014 Revised: 4 Aug. 2014
Accepted: 11 Oct. 2014
*Corresponding author:
V. Behjat (E-mail: behjat@azaruniv.ac.ir)

required which consequences declining of the performance quality [7-9]. Several trials [7-12] have been reported in the literature to present advantages of using axial flux PM synchronous generator (AFPMSG) in wind turbines.

The iron core used in AFPMGS increase the weight of the machine. In addition, there are large axial forces between the permanent magnet rotor and the iron core, which must be regulated carefully during assembly. An alternative solution is to hold the axial flux topology with an air-cored armature structure with concentrated armature coils [13], [14]. A coreless AFPM can operate at higher efficiency than traditional machines because of the absence of the core losses. Adoption of ironless windings results in a considerable reduction in the stator weight. In addition, the cogging torque would be eliminated by using an ironless stator. This paper presents 3D FEM analysis of an air-cored axial flux permanent magnet synchronous generator for low speed, direct drive applications. Although, Refs. [13, 15] are also dealing with air-cored axial flux AFPMSG applications, the authors of this study try to obtain more performance characteristics and evaluate the structure in larger in view of voltage and size. This paper also presents experimental tests on a system realized in the laboratory.

The paper is organized as follows; Section 2 introduces the topology and structure of the proposed generator considered in this study. Three dimensional Finite Element Modeling (FEM) of the machine is explained in Section 3. Section 4 addresses the experimental system realized in the laboratory. Section 5 illustrates the results of the FEM analysis and experimental tests. Finally, conclusions will be given in the last section.

2. MACHINE STRUCTURE

The considered machine is a double-rotor single-stator axial-flux permanent magnet synchronous generator. Fig. 1(a) shows the presented generator structure, consisting of one stator and two rotor parts. Ironless stator winding is located in the air gap between the rotor discs. Circular flat-shaped high-energy Neodymium-Iron-Boron (Nd-Fe-B) magnets are mounted on surfaces of the solid-iron rotor disk. The rotor discs are constructed of steel S232JR structure, and supporting parts. Air-core windings are kept in position by non-magnetic non-conducting stator disc, rather than iron slots. Absent stator teeth and back-iron yoke results in elimination of the cogging torque and iron losses, axial magnetic forces between the rotor and stator, and easier assembly. This form of AFPM generator is considered as a high-efficiency machine. The magnets on each rotor disc are directly aligned with an opposite pole in the structure. In the North-South (NS) topology, the main flux flows from one rotor to another rather than travels circumferentially along stator core and decrease the necessity of stator yoke. Rotor discs and arranged pole magnets are shown in Fig. 1(b).

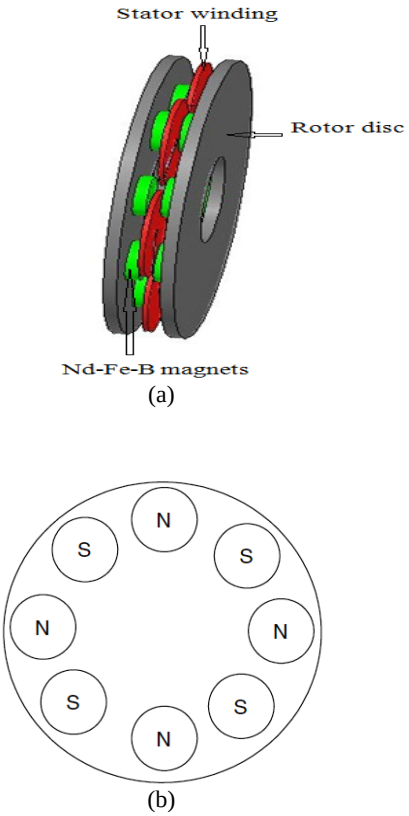

Fig. 1. Proposed machine, (a) coreless double-rotor single-stator (AFPMSG), (b) arrange of Nd-Fe-B magnets.

Flux paths in the machine are shown in Fig. 2. As shown in Fig. 2, the flux in the rotor core (Φ_r) is half of the pole flux in the air gap (Φ_g). Rotor core thickness (l_r) can be calculated using flux equality and known parameters as follows [13]:

$$\Phi_g = B_g A_g \quad (1)$$

$$A_g = \frac{\pi R_m^2}{P} \quad (2)$$

$$\phi_r = \frac{\phi_g}{2} = \frac{B_{br} A_r}{2} \quad (3)$$

$$l_r = \frac{A_r}{R_O - R_i} \quad (4)$$

where, R_O, R_i, R_m, B_{br} and P are the outer radius of the rotor, inner radius of the rotor, radius of the magnet, rotor back core flux density and number of poles, respectively.

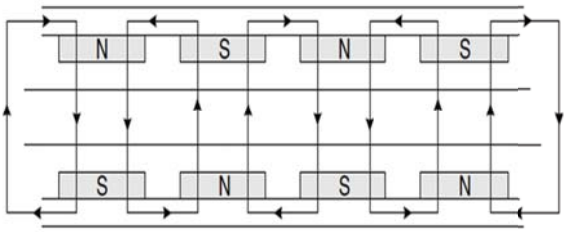

Fig. 2. Flux paths in the machine.

Permanent magnets and concentrated armature coils are circular, because they are simple to fabricate and assemble, also nearly sinusoidal voltage is produced in output of the machine. Concentrated armature coils of the stator are glued on a bony fiber that is non-magnetic material and resistive against thermal variations. To calculate the induced voltage, the variation of flux in the coils is assumed sinusoidal. The induced voltage in each phase of the stator terminal is expressed as:

$$V_{coil} = \frac{d\lambda}{dt} = \lambda_{\max} \cos(\omega t) \quad (5)$$

$$\lambda_{\max} = N \iint B_y(r,\theta) r dr d\theta \quad (6)$$

where, $\lambda_{\max}$, B_y and N are the flux linkage, magnetic flux density in middle of the air gap, and number of coil turns, respectively. It is clear that:

$$0 \le r \le 0.5(r_o + r_i) \quad (7)$$

where, r_o and r_i are the inner and outer radius of the armature coils. The induced voltage in each phase is obtained as below:

$$V_{ph} = \sqrt{2}\, \pi\, f\, \Phi_{ph} N_{ph} \cos(\omega t) \quad (8)$$

Where, V_{ph}, f, Φ_{ph} and N_{ph} are output phase voltage of the generator, output frequency, magnetic flux per pole and number of coil turns in series per phase, respectively. By using circular shape magnets and coils, maximum voltage, minimum winding resistance and inductance can be achieved. The required number of the concentrated coils N_{coil} is calculated by:

$$N_{coil} = \frac{3}{4}(2P) \quad (9)$$

In the above equation, P is the number of pole pairs. The resistance of each coil is obtained as follows:

$$R_{coil} = \rho \frac{N_{coil}\, 2\pi\, r_{cm}}{a_{cs}} \quad (10)$$

$$r_{cm} = \frac{r_i + r_o}{2} \quad (11)$$

where, a_{cs} is the wire cross-sectional area and r_{cm} is the mean radius of the coil. The resistance of the winding per phase is obtained as:

$$R_s = \frac{N_{s,phase}}{N_{coil}} R_{coil} \quad (12)$$

where, $N_{s,phase}$ is the total number of turns of the coils in series per phase. The inductance of each coil is obtained as follows:

$$L_{coil} = k_L \Lambda \quad (13)$$

$$\Lambda = \mu_0 \frac{N_{coil}^2 \pi r_i^2}{g} + \mu_o \frac{N_{coil}^2 \pi}{g(r_0 - r_i)^2} \Pi \quad (14)$$

$$\Pi = \frac{r_o^4}{6} - r_o^2 r_i^2 + \frac{4 r_i^2 r_o}{2} - \frac{r_i^4}{2} \quad (15)$$

where, $k_L = 1.2$, and per phase inductance value is obtained as follows:

$$L_s = \frac{N_{s,phase}}{N_{coil}} L_{coil} \quad (16)$$

The design parameters of the constructed generator are listed in Table 1.

3. FE MODELIG

The presented AFPM has to be modeled in 3-D FEA environment due to its 3-D flux distribution. In the three-dimensional (3D) problem considered here for the electromagnetic analysis of the studied

AFPMSG, the electromagnetic field and circuit-coupled approach based on the A-V-A formulation is used. From the well-known Maxwell's equations, the computation of the magnetic field, based on the A-V-A formulation with the Coulomb gauge, leads to the following equation [16]:

$$\nabla\times\left([v]\nabla\times\vec{A}\right)-\nabla v_e\nabla.\vec{A}=\vec{J} \tag{17}$$

$$-\nabla.[\sigma]\left(\frac{\partial\vec{A}}{\partial t}+\nabla V\right)=\nabla.J=0 \tag{18}$$

The governing equation in the permanent magnet region is described as follows:

$$\nabla\times\left([v]\nabla\times\vec{A}\right)-\nabla v_e\nabla.\vec{A}=\nabla\times\left(\frac{[v][\overrightarrow{M_0}]}{v_0}\right) \tag{19}$$

where, $\vec{A}$ and V are the magnetic vector potential and scalar electric potential, respectively. $[v]$ is the reluctivity matrix and $[\sigma]$ is the conductivity matrix. v_e is defined as one-third of the reluctivity matrix. $\vec{J}$ is the current density, $\overrightarrow{M_0}$ is the remanent intrinsic magnetization vector and v_0 is the reluctivity of the free space. Full meshed model of the considered generator is illustrated in Fig. 3.

Table 1. Design parameters of the constructed machine.

Parameters	Value
N_{coil}	300
$N_{s,phase}$	600
Electrical power (w)	300
Number of poles	8
Number of coils	6
Number of phases	3
Radius of circular magnet	25 (mm)
Distance between center of discs and permanent magnets	100 (mm)
Inner radius of coil	6 (mm)
outer radius of coil	115 (mm)
Permanent Magnet Axial Length	10 (mm)
Air gap between permanent magnets	20 (mm)
Thickness of back iron	10 (mm)
Speed	600 (rpm)
Axial length of generator	60 (mm)
Outer radius of back iron disc	150 (mm)
Permanent Magnet Residual Flux Density	1.20 (T)

The number of nodes, line elements, surface elements and volume elements of the developed FEM model are listed in Table 2.

Table 2. FEM meshed model characteristics.

Number of nodes	48053
Number of elements	7113
Number of surface elements	86046
Number of volume elements	202525

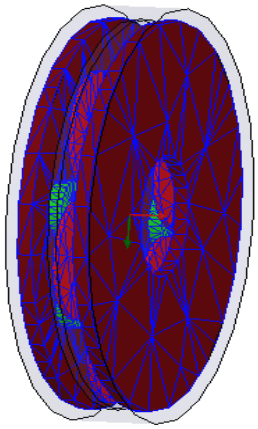

Fig. 3. FEM result: meshed model of the proposed generator.

The value of the flux density in various parts of the machine is an important and effective parameter in both core losses and the amount of saturation to which the machine is exposed. The revelation of the varying flux density at various machine parts is studied using the developed FEM model. Fig. 4(a) presents the magnetic flux density distribution in the generator. Fig. 4(b) and 4(c) illustrate magnetic flux density values in back iron and PMs of the considered machine. It is observed that the maximum flux density in back iron is 1.2 *T* which is appropriate value of flux density and lower than the field saturation value of the magnetic iron. Air gap magnetic flux density is shown in Fig. 4(d), where the amount of flux density value is (0.7 *T*). It is observed that the magnetic flux density values are acceptable and suitable.

4. EXPERIMENTAL SETUP

According to the main specifications and dimensions given in Table 1, the case study AFPMSG has been constructed and tested in order

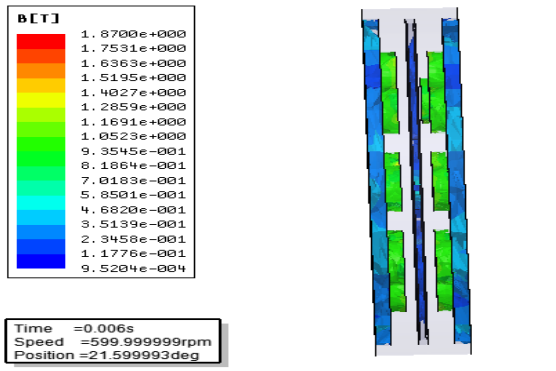

(a)

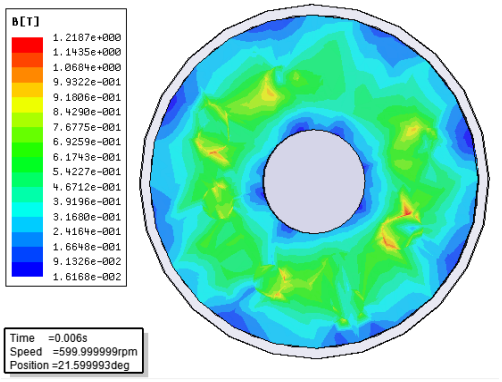

(b)

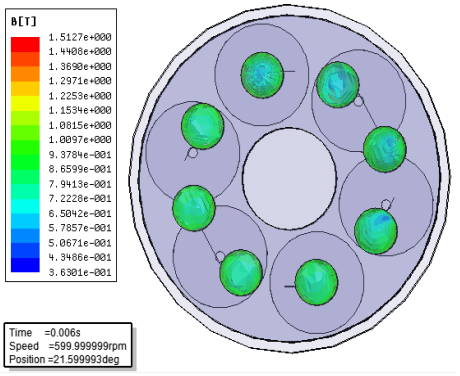

(c)

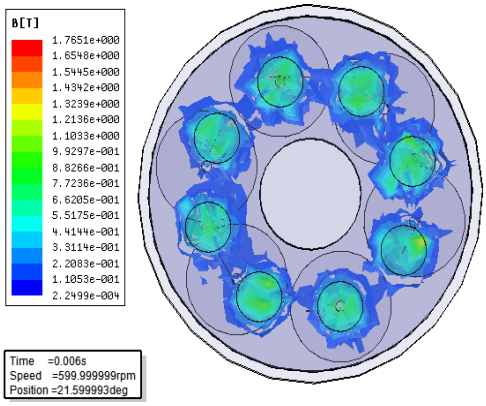

(d)

Fig. 4. Magnetic flux density distribution in the: (a) all generator parts, (b) back iron, (c) PMs, (d) Air gap.

to demonstrate the possibility of experimental tests of the proposed solution. The machine was driven by an induction motor fed by a frequency converter and loaded with a resistive load bank. Under load conditions, the most important effect of the armature reaction field in surface of the permanent magnets is the possibility of partially or totally demagnetizing of the magnets. The stator of the constructed AFPMSG can be seen in Fig. 5 (a). Windings are connected electrically in star connection. Fig. 5(b) shows in detail the rotor discs of the machine. The completed generator is shown on the laboratory test bench in Fig. 5 (c).

(a)

(b)

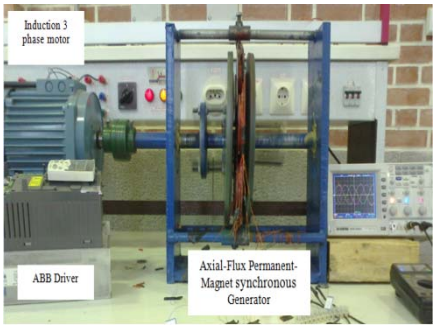

(c)

Fig. 5. (a) Detailed structure of the rotor discs, (b) Winding coil of the stator, (c) Experimental setup and case study generator.

Each of the phase coils includes 300 turns and the total number of phase turns is then 600. Both ends of the phase windings are available in a connection box. As a result, renders possible changing of the machine's electrical connection from star to delta.

5. FEM AND EXPERIMENTAL RESULTS

The no-load phase voltage of the generator with 600 rpm shaft speed is shown in Fig. 6, while the two armature coils in each phase are connected in series. The corresponding experimental results, for the same conditions with FEM analysis, are shown in Fig. 7. The voltage signals with approximately 60-V of peak value for both sets of results proves the accuracy of the model.

Figure 8(a) indicates the voltage signals obtained from the experimental tests where a 3 phase R-L load ($R = 15\Omega, \mathrm{L} = 68$ mH) is connected to the machine. Fig. 8 (b) shows one phase voltage and load current.

Figure 9 illustrates the line-to-neutral voltage with respect to the load current of the machine. As it is obvious from the figure, a low voltage drop is seen between the no load and full load conditions.

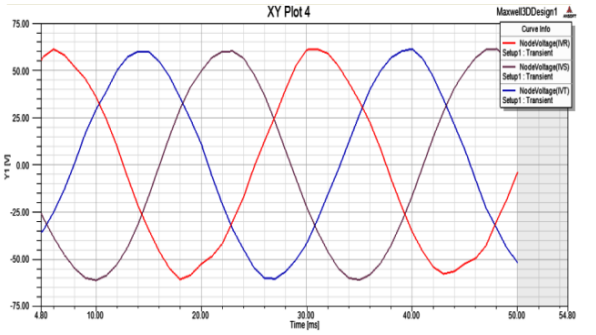

(a)

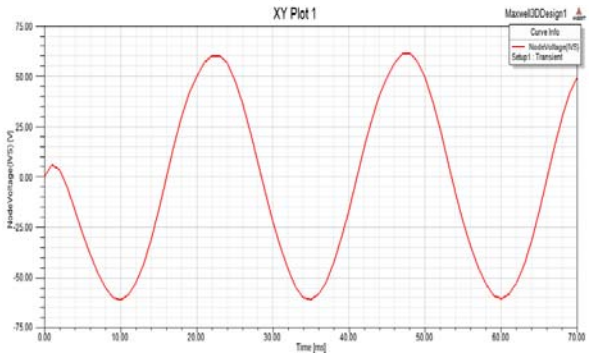

(b)

Fig. 6. 3-D FEM, no-load voltage at 600 r/min: (a) 3 phase, (b) one phase.

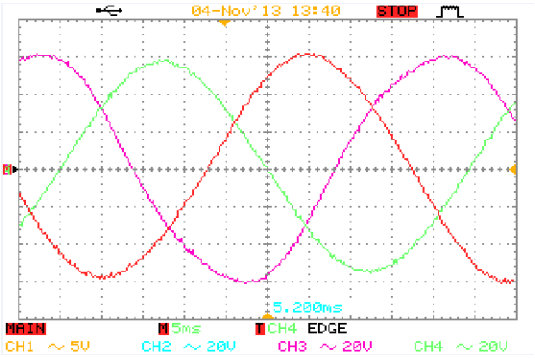

(a)

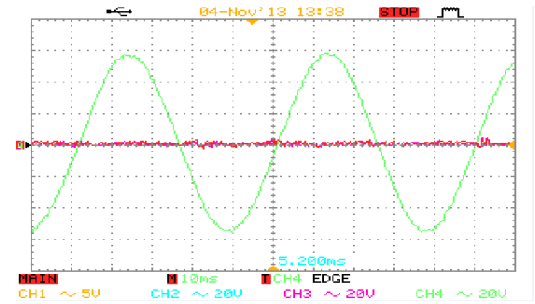

(b)

Fig. 7. Experimental, no-load voltage at 600 r/min: (a) 3 phase, (b) one phase.

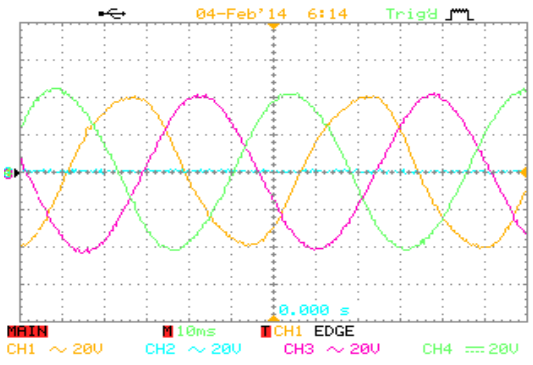

(a)

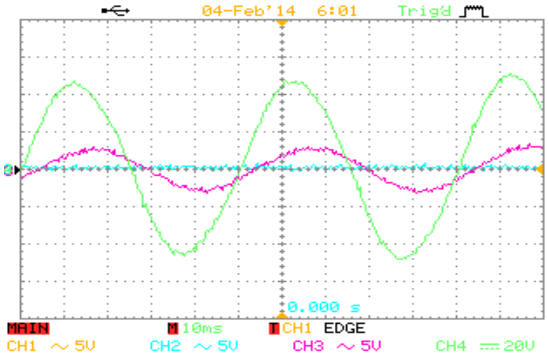

(b)

Fig. 8. Experimental test, (R-L load connected to the machine) at 600 r/min: (a) 3 phase load voltage, (b) one phase voltage and load current.

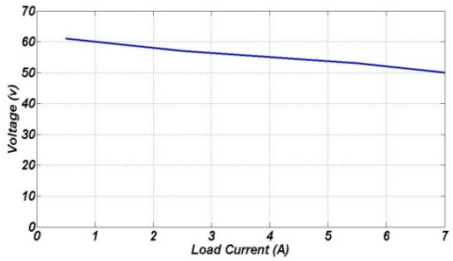

Fig. 9. FEM output voltage amplitude versus load current at 600 r/min.

No-load test of the machine was also performed with variable speed condition. Figure 10 illustrates the relation between the induced voltage and speed of the machine in both of the simulation and experimental tests. It is easily observed that a linear relation exists between the voltage and speed of the rotor.

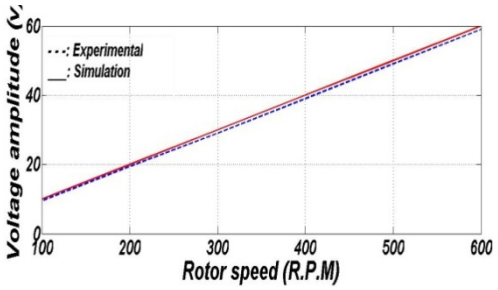

Fig. 10. FEM and experimental output voltage versus variable speed of the machine.

As it has been depicted in the given results from Fig. 6 to Fig. 10, the output voltage of the machine is nearly sinusoidal in low speed operation and has linear relation with the rotor speed. Therefore, the output voltage of the constructed AFPMSG is controllable and can be regulated easily. These characteristics of the suggested topology make it suitable for wind turbine application. Future work ought to focus on other aspects of the machine like dynamic modeling of the machine and detailed consideration of the efficiency. In addition, more exhaustive tests on the constructed AFPMSG is highly desirable in the future works to establish more reliable machine for wind turbine applications.

6. CONCLUSIONS

This research work presented performance evaluation of an air-cored slotless axial flux permanent magnet synchronous generator, which is suitable for low speed applications such as wind turbines. Simple structure, and low cost are the main advantages that achieved. The simulation and experimental test results on a system realized in the laboratory proved that the considered generator has a sinusoidal output voltage in low speed operation, which is a linear function of the speed. FEM analysis results were depicted proper distribution of the electromagnetic flux on various parts of the machine. All these characteristics of the suggested topology make it suitable for wind turbine application.

REFERENCES

[1] S.M. Dehghan, M. Mohamadian, and A.Y. Varjani, “A new variable-speed wind energy conversion system using permanent-magnet synchronous generator and Z-source inverter,” *IEEE Transactions on Energy Conversion*, vol. 24, no. 3, pp.714-724, 2009.

[2] S. Zhang, K.-J. Tseng, D. M. Vilathgamuwa, T. D. Nguyen and X.-Y. Wang, “Design of a robust grid interface system for PMSG-based wind turbine generators,” *IEEE Transactions on Industrial Electronics*, vol. 58, no. 1, pp. 316-328, 2011.

[3] C. H. Ng, M. A. Parker, L. Ran, P. J. Tavner, J. R. Bumby and E. Spooner, “A multilevel modular converter for a large, light weight wind turbine generator, ” *IEEE Transactions on Power Electronics*, vol. 23, no. 3, pp. 1062-1074, 2008.

[4] Z. Chen, J. M. Guerrero and F. Blaabjerg, “A review of the state of the art of power electronics for wind turbines,” *IEEE Transactions on Power Electronics*, vol. 24, no. 8, pp. 1859-1875, 2009.

[5] J.M. Carrasco, L.G. Franquelo, J.T. Bialasiewicz, E. Galvan, R. C. P. Guisado, A. M. Prats, J.I. Leon and N. Moreno-Alfonso, “Power electronic systems for the grid integration of renewable energy sources: A survey,” *IEEE Transactions on Industrial Electronics*, vol. 53, no. 4, pp. 1002-1016, 2006.

[6] H. Polinder, F.F. A. Van de Pijl, G.-J. de Vilder

and P.J. Tavner, “Comparison of direct drive and geared generator concepts for wind turbines,” *IEEE Transactions on Energy Conversion*, vol. 21, no. 3, pp. 725-733, 2006.

[7] B. Wu, Y. Lang, N. Zargari and S. Kouro, “Power conversion and control of wind energy systems,” Wiley-IEEE Press, 2011.

[8] A. D. Gerlando, G. Foglia, M.F. Iacchetti and Roberto Perini, “Axial flux PM machines with concentrated armature windings: design analysis and test validation of wind energy generators”, *IEEE Transactions on Industrial Electronics*, vol. 58, no. 9, pp. 3795-3805, 2011.

[9] M. Aydin, S. Huang and T.A. Lipo, “Axial flux permanent magnet disc machines: A Review”, *Wisconsin Electric Machines and Power Electronics Consortium*, pp. 1-11, 2004.

[10] M. Lin, L. Hao, X. Li, X. Zhao and Z.Q. Zhu, “ A novel axial field flux-switching permanent magnet wind power generator”, *IEEE Transactions on Magnetics*, vol. 47, no. 10, pp. 4457 - 4460, 2011.

[11] S. Brisset, D. Vizireanu and P. Brochet, “Design and optimization of a nine-phase axial-flux PM synchronous generator with concentrated winding for direct-drive wind turbine”, *IEEE Transactions on Industrial Applications*, vol. 44, no. 3, pp. 707-715, 2008.

[12] Y.-S. Park , S.-M. Jang , J.-H. Choi , J.-Y. Choi and D.-J. You, “Characteristic analysis on axial flux permanent magnet synchronous generator considering wind turbine characteristics according to wind speed for small-scale power application”, *IEEE Transactions on Magnetics*, vol. 48, no. 11, pp. 2937 – 2940, 2012.

[13] J.R. Bumby and R. Martin, “Axial-flux permanent-magnet air-cored generator for small-scale wind turbines”, *IET Electric Power Applications*, vol. 152, no.5, pp. 1065 -1075, 2005.

[14] M.J. Kamper, R.J. Wang, and F.G. Rossouw, “Analysis and performance of axial flux permanent-magnet machine with air-core non overlapping concentrated stator windings,” *IEEE Transactions on Industrial Applications*, vol. 44, no. 5, pp. 1495-1504, 2008.

[15] S. Javadi and M. Mirsalim, “Design and analysis of 42-V coreless axial-flux permanent-magnet generators for automotive applications,” *IEEE Transactions on Magnetics*, vol. 44, no. 5, pp. 1495-1504, 2008.

[16] T.F. Chan, W. Wang and L.L. Lai, “Performance of an axial-flux permanent magnet synchronous generator from 3-D finite-element analysis”, *IEEE Transactions on Energy Conversion*, vol. 25, no. 3, pp. 669 – 676, 2010.